Front. Phys. 13(2), 130307 (2018)
https://doi.org/10.1007/s11467-017-0732-4

RESEARCH ARTICLE

Stationary and moving solitons in spin–orbit-coupled spin-1 Bose–Einstein condensates

Yu-E Li, Ju-Kui Xue†

Key Laboratory of Atomic Molecular Physics & Functional Materials of Gansu Province, College of Physics and Electronic Engineering, Northwest Normal University, Lanzhou 730070, China
Corresponding author. E-mail: †xuejk@nwnu.edu.cn
Received June 10, 2017; accepted September 28, 2017

We investigate the matter-wave solitons in a spin–orbit-coupled spin-1 Bose–Einstein condensate using a multiscale perturbation method. Beginning with the one-dimensional spin–orbit-coupled three-component Gross–Pitaevskii equations, we derive a single nonlinear Schrödinger equation, which allows determination of the analytical soliton solutions of the system. Stationary and moving solitons in the system are derived. In particular, a parameter space for different existing soliton types is provided. It is shown that there exist only dark or bright solitons when the spin–orbit coupling is weak, with the solitons depending on the atomic interactions. However, when the spin–orbit coupling is strong, both dark and bright solitons exist, being determined by the Raman coupling. Our analytical solutions are confirmed by direct numerical simulations.

Keywords spin–orbit coupling, Bose–Einstein condensate, soliton, perturbation method

PACS numbers 03.75.Mn, 03.75.Ss, 03.75.Kk

1 Introduction

Bose–Einstein condensates (BECs) have become a significant platform for exploring non-linear coherent structures. A large number of coherent structures have successfully been discovered, such as vortices [1], Anderson localization of matter waves [2, 3], dark and bright solitons, and ring dark solitons [4–11]. Developments concerning two-component BECs have further expanded this research field. Two-component BECs offer a greater number of tunable parameters than single-component cases and also incorporate richer coherent structures, including dark-bright complexes [12–15], domain walls [16, 17], vortex-antivortex dipoles [18–20], and skyrmions [21, 22].

In particular, the experimental realization of spin–orbit coupling (SOC) in spin-$\frac{1}{2}$ condensate by the National Institute of Standards and Technology (NIST) group has motivated many theoretical studies on SOC BECs [23]. These studies have included investigations of vortex structures in rotating SOC BECs [25–27], zitterbewegung, the quantum spin Hall effect, and soliton excitation [28–30]. Most notably, localized modes in repulsive and attractive SOC BECs have been investigated [31]. Through use of a multiscale expansion method, three types of bright solitons have been discovered in SOC attractive BECs, each having zero momentum, finite momentum, or stripe densities [32]. Pertinent research has also revealed the "negative mass soliton" regimes [33], in which corresponding "negative mass" bright or dark solitons can exist for repulsive or attractive interactions, respectively. In addition, solitons in one-dimensional (1D), 2D, and 3D SOC BECs have been demonstrated [34–39]. Very recently, coupling between atomic spin and its momentum was experimentally achieved in a spin-1 ^{87}Rb condensate [40]. This high-spin system has drawn considerable attention in both theoretical and experimental studies of SOC spin-1 condensates. Further, the ground-state structure [41], phase separation [42], and the phase transition and elementary excitation [43] in a SOC spin-1 condensate have been predicted and studied. In particular, multi-peak bright solitons [44] and bright single- and multi-peak vector solitons [45] have been found in SOC spin-1 BECs.

In this paper, we report a study of matter-wave solitons in SOC spin-1 BECs using a multiscale perturbation method. This method allows derivation of a single nonlinear Schrödinger (NLS) equation from the SOC three-component Gross–Pitaevskii (GP) equations. Applying

this NLS equation, we find different types of solitons, including stationary dark and bright solitons and moving dark and bright solitons, and also present the parameter regions for the existing dark and bright solitons. The soliton types are determined by the coupled effects of the SOC, Raman coupling, and atomic interaction. We verify our analytical stationary and moving soliton solutions via numerical simulations.

2 Model and derivation of NLS equation

We consider a spin-1 SOC spinor BEC confined in a quasi-1D trap, for which the trapping frequencies along the y and z axes (ω_y and ω_z) are considerably stronger than that along the x axis (ω_x). The single-particle Hamiltonian of the system is

$$H_0 = \frac{p_x^2}{2m} + \gamma p_x \Sigma_z + \Omega_0 \Sigma_x, \tag{1}$$

where $p_x = -\mathrm{i}\hbar\partial_x$ is the momentum operator along the x axis. Here, $\gamma = \hbar k_r/m$ is the strength of the Raman laser that couples the two hyperspin components of the ^{87}Rb hyperfine state, with k_r being the Raman laser wavenumber and m being the atomic mass. Ω_0 is the Rabi frequency, and Σ_z and Σ_x is the matrix representations of the z and x components of the spin-1 angular momentum operator, respectively, where

$$\Sigma_z = \begin{pmatrix} 1 & 0 & 0 \\ 0 & 0 & 0 \\ 0 & 0 & -1 \end{pmatrix}, \quad \Sigma_x = \frac{1}{\sqrt{2}} \begin{pmatrix} 0 & 1 & 0 \\ 1 & 0 & 1 \\ 0 & 1 & 0 \end{pmatrix}. \tag{2}$$

Considering the interactions in the Hartree approximation and using the single-particle model Hamiltonian (1), we can state that a quasi-1D spin-1 BEC is governed by the following three coupled dimensionless GP equations for the wave functions ψ_j (with $j = 1, 0, -1$):

$$\begin{aligned} \mathrm{i}\frac{\partial\psi_1}{\partial t} = &\left(-\frac{1}{2}\frac{\partial^2}{\partial x^2} + V + c_0\rho\right)\psi_1 + c_2(\rho_1+\rho_0-\rho_{-1})\psi_1 \\ &+ c_2\psi_{-1}^*\psi_0^2 - \mathrm{i}\gamma\frac{\partial\psi_1}{\partial x} + \Omega\psi_0, \end{aligned} \tag{3}$$

$$\begin{aligned} \mathrm{i}\frac{\partial\psi_0}{\partial t} = &\left(-\frac{1}{2}\frac{\partial^2}{\partial x^2} + V + c_0\rho\right)\psi_0 + c_2(\rho_1+\rho_{-1})\psi_0 \\ &+ 2c_2\psi_1\psi_{-1}\psi_0^* + \Omega(\psi_1+\psi_{-1}), \end{aligned} \tag{4}$$

$$\begin{aligned} \mathrm{i}\frac{\partial\psi_{-1}}{\partial t} = &\left(-\frac{1}{2}\frac{\partial^2}{\partial x^2} + V + c_0\rho\right)\psi_{-1} + c_2(\rho_{-1}+\rho_0-\rho_1)\psi_{-1} \\ &+ c_2\psi_1^*\psi_0^2 + \mathrm{i}\gamma\frac{\partial\psi_{-1}}{\partial x} + \Omega\psi_0, \end{aligned} \tag{5}$$

where $c_0 = 2Nl_0(a_0+2a_2)/(3l_{yz}^2)$, $c_2 = 2Nl_0(a_2-a_0)/(3l_{yz}^2)$, a_0 and a_2 are the s-wave scattering lengths in the total spin 0 and 2 channels, respectively, and $l_0 = \sqrt{\hbar/(m\omega_x)}$ is the oscillator length along the x axis. Further, $l_{yz} = \sqrt{\hbar/(m\omega_{yz})}$, where $\omega_{yz} = \sqrt{\omega_y\omega_z}$ is the oscillator length in the y-z plane. In addition, the $\rho_j = |\psi_j|^2$ (with $j = 1, 0, -1$) are the component densities, while $\rho = \sum_{i=-1}^{1}|\psi_j|^2$ is the total density and $V = x^2/2$ is the 1D harmonic trap. Further, $\gamma = k_r\sqrt{\hbar/(m\omega_x)}$ and $\Omega = \Omega_0/(\sqrt{2}\hbar\omega_x)$. Here, time, length, and energy are measured in units of ω_x^{-1}, l_0, and $\hbar\omega_x$, respectively, and N is the total number of atoms. Based on experiments on ^{87}Rb [23, 24, 40] and for $\omega_x = 2\pi\times 20$ Hz, $\omega_y = \omega_z = 2\pi\times 400$ Hz, $\lambda_L \equiv 2\pi/k_r = 1064$ nm (where λ_L is the Raman laser wavelength), and the Ω_0 parameters in the range of $(1-10)E_L$ with $E_L = \hbar^2k_r^2/(2m)$, we can estimate $\gamma \sim 10$ and $\Omega \sim 100$. Note that the atomic interactions c_0 and c_2 can be adjusted from attractive to repulsive using the Feshbach resonance technique.

Next, we reduce the system of Eqs. (3)–(5) to a single NLS equation via a multiscale perturbation method [33]. This method allows determination of the dark and bright solitons for different SOC and Raman coupling parameter regions. In this work, for a sufficiently weak trap, we consider the homogeneous case only, i.e., $V = 0$.

We seek solutions to Eqs. (3)–(5) of the form

$$\Psi = \sum_{n=1}^{\infty}\epsilon^n\boldsymbol{u}_n\mathrm{e}^{\mathrm{i}(kx-\mu t)} \equiv \sum_{n=1}^{\infty}\epsilon^n\begin{pmatrix} U_n \\ V_n \\ W_n \end{pmatrix}\phi_n\mathrm{e}^{\mathrm{i}(kx-\mu t)}, \tag{6}$$

where $\Psi = (\psi_1, \psi_0, \psi_{-1})^T$ and the vectors $\boldsymbol{u}_n = [U_n, V_n, W_n]^T\phi_n$. Here, U_n, V_n, and W_n with $n = 1, 2, 3$ are the coefficients of unknown field envelopes $\phi_n \equiv \phi_n(T, X)$, which are functions of the slow variables $T = \epsilon^2 t$ and $X = \epsilon(x - vt)$. Here, ϵ is a small parameter ($\epsilon \ll 1$) and v is the group velocity. In addition, k is the momentum, $\mu = \omega + \epsilon^2\varpi$ is the chemical potential, ω is the energy in the linear regime, and $\epsilon^2\varpi$ is a small energy deviation about this energy.

Substituting Eq. (6) into Eqs. (3)–(5), we obtain these equations at $O(\epsilon)$, $O(\epsilon^2)$, and $O(\epsilon^3)$, respectively:

$$\boldsymbol{M}\boldsymbol{u}_1 = 0, \tag{7}$$

$$\boldsymbol{M}\boldsymbol{u}_2 = \mathrm{i}\boldsymbol{M}_0\partial_X\boldsymbol{u}_1, \tag{8}$$

$$\boldsymbol{M}\boldsymbol{u}_3 = \mathrm{i}\boldsymbol{M}_0\partial_X\boldsymbol{u}_2 - \left(\mathrm{i}\partial_T + \frac{1}{2}\partial_X^2 - \boldsymbol{G} + \varpi\right)\boldsymbol{u}_1, \tag{9}$$

where matrices $\boldsymbol{M}$ and $\boldsymbol{M}_0$ are defined as follows:

$$\boldsymbol{M} = \begin{pmatrix} \omega - \frac{1}{2}k^2 - k\gamma & -\Omega & 0 \\ -\Omega & \omega - \frac{1}{2}k^2 & -\Omega \\ 0 & -\Omega & \omega - \frac{1}{2}k^2 + k\gamma \end{pmatrix}, \tag{10}$$

$$\boldsymbol{M}_0 = \begin{pmatrix} v - k - \gamma & 0 & 0 \\ 0 & v - k & 0 \\ 0 & 0 & v - k + \gamma \end{pmatrix}. \tag{11}$$

For matrix $\boldsymbol{G}$, $\boldsymbol{G}_{ij} = 0$ $(i \neq j)$, $\boldsymbol{G}_{11} = (A + B - c_2 V_1^2 \frac{W_1}{U_1})|\phi_1|^2$, $\boldsymbol{G}_{22} = (A + E - 2c_2 U_1 W_1)|\phi_1|^2$, and $\boldsymbol{G}_{33} = (A + D - c_2 V_1^2 \frac{U_1}{W_1})|\phi_1|^2$, where $A = c_0(U_1^2 + V_1^2 + W_1^2)$, $B = c_2(U_1^2 + V_1^2 - W_1^2)$, $D = c_2(W_1^2 + V_1^2 - U_1^2)$, and $E = c_2(U_1^2 + W_1^2)$.

At $O(\epsilon)$, Eq. (7) indicates that the solvability condition $\det(\boldsymbol{M}) = 0$ yields the linear excitation energy spectrum

$$\omega_\pm(k) = \frac{1}{2}k^2 \pm \sqrt{k^2\gamma^2 + 2\Omega^2}, \tag{12}$$

$$\omega_0(k) = \frac{1}{2}k^2. \tag{13}$$

Eqs. (12) and (13) correspond to the linear excitation energy spectrum, which consists of three different bands, namely, upper ($\omega_+(k)$), lower ($\omega_-(k)$), and intermediate ($\omega_0(k)$). Below, we investigate nonlinear states in the form of solitons, which correspond to the lower energy band. Note that the lower branch $\omega_-(k)$ has different behaviors depending on the sign of the parameter $\Delta \equiv 1 - 2\Omega^2/\gamma^4$. That is, when $\Delta < 0$ $(\Omega/\gamma^2 > \sqrt{2}/2)$, $\omega_-(k)$ has one minimum at $k = 0$. However, when $\Delta > 0$ $(\Omega/\gamma^2 < \sqrt{2}/2)$, $\omega_-(k)$ has two minima at $k = \pm k_0 = \pm\sqrt{\gamma^2 + \frac{2\Omega^2}{\gamma^2}}$. Then, the first-order equation [Eq. (7)] has the solution

$$\boldsymbol{u}_1 = \begin{pmatrix} U_1 \\ V_1 \\ W_1 \end{pmatrix} \phi_1(X,T) = \begin{pmatrix} 1 \\ Q \\ Q^2/2 \end{pmatrix} \phi_1(X,T), \tag{14}$$

where the parameter Q is given by

$$Q = \left(\omega - \frac{1}{2}k^2 - k\gamma\right)/\Omega. \tag{15}$$

Note that the above parameter sets the left and right eigenvectors of $\boldsymbol{M}$ at eigenvalue 0, being given by $\boldsymbol{L} = [1, Q, Q^2/2]$ and $\boldsymbol{R} = [1, Q, Q^2/2]^T$, respectively.

At $O(\epsilon^2)$, the compatibility condition of Eq. (8), i.e., $\boldsymbol{L}\boldsymbol{M}_0\boldsymbol{R} = 0$, yields

$$v = \left[\left(\Omega^2 - \omega\gamma - \frac{1}{2}k^2\gamma\right)Q^2 + 2\Omega\left(k - \omega + \frac{1}{2}k^2\right)Q + 2\left(\Omega^2 + (k+\gamma)\left(\omega - \frac{1}{2}k^2\right)\right)\right] \Big/ (2\omega - k^2 - k\gamma Q^2 + 2\Omega Q). \tag{16}$$

Here, it is apparent that v is determined by three parameters, i.e., the Raman coupling Ω, SOC γ, and k. Using Eq. (14), we can obtain the solutions of Eq. (8), where

$$\boldsymbol{u}_2 = -i \begin{pmatrix} 1 \\ Q + \frac{1}{\Omega}(v - k - \gamma) \\ Q^2/2 + \frac{2k\gamma(v-k) - 2\gamma(\omega - \frac{1}{2}k^2)}{(\omega - \frac{1}{2}k^2 + k\gamma)^2} \end{pmatrix} \frac{\partial \phi_1}{\partial X}. \tag{17}$$

Finally, we consider $O(\epsilon^3)$. Taking advantage of the compatibility condition for Eq. (7), i.e., $\det(\boldsymbol{M}) = 0$, together with Eqs. (14) and (17), we eliminate the third-order terms $\boldsymbol{u}_3$ from Eq. (9) and obtain an NLS equation for the unknown field envelope $\phi_1 = \phi$:

$$\mathrm{i}\frac{\partial \phi}{\partial T} = -\frac{1}{2}P\frac{\partial^2 \phi}{\partial X^2} + S|\phi|^2\phi - \varpi\phi. \tag{18}$$

Here, the coefficients are given by

$$P = (1 + 2k - 2v) + [((v-k+\gamma)(2k\gamma v - 2\gamma\omega - k^2\gamma) + 2\gamma\Omega^2)Q^4 + 8\Omega(v-k)(v-k-\gamma)Q - 8\gamma\Omega^2]/(4\Omega^2 + 4\Omega^2Q^2 + \Omega^2Q^4),$$

$$S = c_0\left(1 + Q^2 + \frac{Q^4}{4}\right) + c_2\left(1 + Q^2 - \frac{Q^4}{4}\right) + 2c_2Q^4(Q^4/4 + \Omega Q^2 + 2\Omega - 1)/(4\Omega + \Omega Q^4 + 4\Omega Q^2).$$

3 Soliton solutions

The above effective NLS equation has soliton solutions. When the signs of the dispersion coefficient P and nonlinearity coefficient S are identical, i.e., $PS > 0$, the solitons are dark. When the signs are opposite, i.e., $PS < 0$, the solitons are bright.

Based on previous investigations [40, 41, 43, 45], we have confirmed that the sign of S mainly relies on the parameters c_0 and c_2, i.e., the atomic interactions. In this paper, we further demonstrate the cases of $S > 0$ and $S < 0$ by choosing two separate sets of c_0 and c_2. Unlike S, the sign of P is determined by the coupled effects of γ, Ω, and k. The dependence of P on k is shown in Fig. 1(a), for $\gamma = 8$ and four different Ω values. It is clearly apparent that, when $\Omega/\gamma^2 > \sqrt{2}/2$ (i.e., when the linear exciting energy spectrum has one minimum), $P > 0$. Thus, two types of soliton can be found for the two cases of (a) $P > 0, S > 0$ and (b) $P > 0, S < 0$. Further, when $\Omega/\gamma^2 < \sqrt{2}/2$ (i.e., when the linear exciting energy spectrum has two minima), there exist intervals of momenta

for $P > 0$ and $P < 0$ simultaneously. Therefore, in this region, we can obtain different types of soliton for the four cases of (a) $P > 0, S > 0$, (b) $P > 0, S < 0$, (c) $P < 0, S > 0$, and (d) $P < 0, S < 0$.

Note that v is also plotted as a function of k in Fig. 1(b). When v is zero, we can obtain stationary solitons; however, when v is nonzero, moving solitons can be obtained. In the $\Omega/\gamma^2 > \sqrt{2}/2$ region, v is zero at a single momentum value, $k = 0$, whereas in the region of $\Omega/\gamma^2 < \sqrt{2}/2$, v is zero for three different momentum values, i.e., 0 and $\pm k_0$. Hence, both stationary and moving solitons can be obtained in both of these cases.

In Fig. 2, dark and bright soliton regions in the (Ω, γ) parameter space are shown for different k. As mentioned above, when $PS > 0$, there exists a dark soliton. However, when $PS < 0$, a bright soliton is obtained. Thus, $PS = 0$ is plotted for different k values in the (Ω, γ) plane in Fig. 2. Note that the regions of dark and bright solitons are opposite for the two cases of $S > 0$ and $S < 0$ (determined by the atomic interaction). Interestingly, when the SOC γ is sufficiently small, only dark $(S > 0)$ or bright $(S < 0)$ solitons appear, depending on the nonlinear coupling constants c_0 and c_2. However, with increased SOC γ, both dark and bright solitons can be obtained at different Raman coupling values (Ω). In that case, stationary and moving dark or bright solitons exist.

We next present various exact soliton solutions of Eq. (18). In the case of $P > 0, S > 0$, with $\varpi > 0$, we obtain the following dark soliton solution of Eq. (18):

$$\phi_d = \sqrt{\varpi/S}(\cos\theta \tanh z_d + \mathrm{i}\sin\theta), \tag{19}$$

where $z_d = \sqrt{\varpi/P}\cos\theta[X - X_0(T)]$. Here, θ is the soliton phase angle, $X_0(T)$ is the soliton center, and the soliton velocity is $\mathrm{d}X_0/\mathrm{d}T = \sqrt{\varpi/P}\sin\theta$.

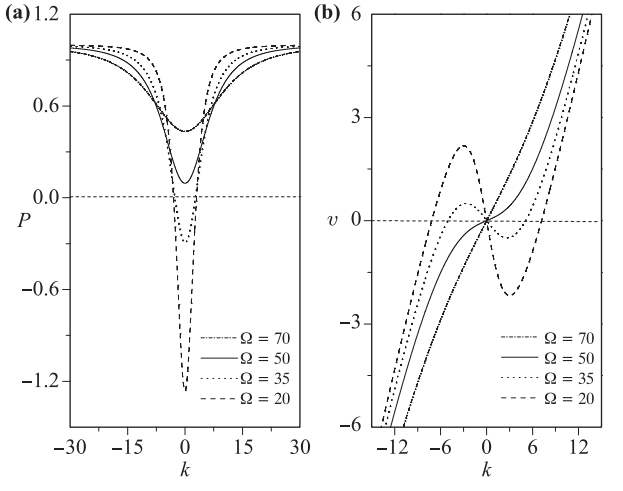

Fig. 1 Analytical profiles of **(a)** dispersion coefficient P and **(b)** group velocity v, for different Raman frequencies Ω and with SOC $\gamma = 8$.

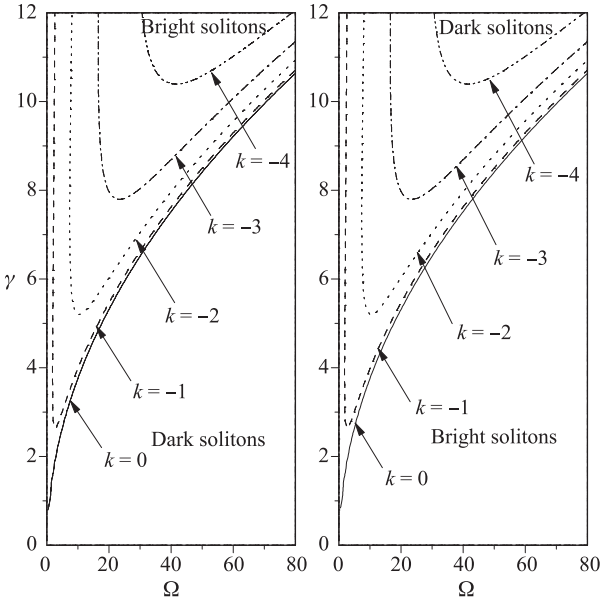

Fig. 2 Dark and bright soliton regions for different k in (Ω, γ) plane. **(a)** $S > 0$ with $c_0 = 1$ and $c_2 = -0.5$. **(b)** $S < 0$ with $c_0 = -1$ and $c_2 = 0.5$.

In the case of $P < 0, S > 0$, with $\varpi < 0$, the bright soliton solution of Eq. (18) is

$$\phi_b = \eta \mathrm{sech} z_b \exp(\mathrm{i}\kappa X), \tag{20}$$

where $z_b = \eta\sqrt{-S/P}[X - X_0(T)]$. Here, η is the soliton amplitude and satisfies the relation $\varpi = (\kappa^2 + \eta^2(-S)/P)[X - X_0(T)]$, where $X_0(T)$ is the soliton center. The soliton velocity is connected to the wavenumber κ, i.e., $\mathrm{d}X_0/\mathrm{d}T = P\kappa$.

We next obtain the first-order approximate soliton solutions of the original Eqs. (3)–(5):

$$\begin{pmatrix}\psi_1\\ \psi_0\\ \psi_{-1}\end{pmatrix} \approx \begin{pmatrix}1\\ Q\\ Q^2/2\end{pmatrix} \epsilon\sqrt{\varpi/S}(\cos\theta\tanh z_d + \mathrm{i}\sin\theta) \times \exp(\mathrm{i}kx - \mathrm{i}(\omega + \epsilon^2\varpi)t), \tag{21}$$

$$\begin{pmatrix}\psi_1\\ \psi_0\\ \psi_{-1}\end{pmatrix} \approx \begin{pmatrix}1\\ Q\\ Q^2/2\end{pmatrix} \epsilon\eta\mathrm{sech} z_b \exp(\mathrm{i}\kappa X) \times \exp(\mathrm{i}kx - \mathrm{i}(\omega - \epsilon^2\varpi)t). \tag{22}$$

Note that Eqs. (21) and (22) are the dark and bright soliton solutions, respectively. Note also that the soliton solutions in the cases of $P > 0, S < 0$ and $P < 0, S < 0$ have the same functional forms as Eqs. (22) and (21), respectively.

Finally, to confirm the above analytical predictions, we adopt the fourth-order Runge–Kutta method to solve the GP Eqs. (3)–(5), with the initial wavefunctions given by Eqs. (21) and (22) at $t = 0$. The solitons for the two cases of $S > 0$ and $S < 0$ have the same properties; therefore, we present examples for the case of $S > 0$ only. The evolutionary profiles of the corresponding stationary and moving solitons are presented in Figs. 3 and 4, respectively. A stationary dark soliton is shown in Figs. 3(a) and (b), while a stationary bright soliton is shown in Figs. 3(c) and (d). In order to obtain these solitons, we selected parameters corresponding to dark or bright solitons with zero v and zero soliton velocity. Interestingly, from Eqs. (15), (21), and (22), the stationary solitons for two different spin components ($m_F = 1$ and -1) have the same amplitudes. These amplitudes are dependent on the k values (when $k = 0$, the amplitudes of the $m_F = 1$ and $m_F = -1$ components are equal) and irrelevant to the values of c_2. Their overlap is apparent in Fig. 3. In addition, the shapes of the stationary solitons do not change during propagation. Note that the solitons are plotted at $t = 0$ and $t = 100$ only.

In Fig. 4, examples of moving solitons at three different times are shown. It is apparent that the solitons propagate without distortion or significant emission of radiation. The moving dark and bright solitons in Fig. 4 travel in opposite directions, because the v values of the dark and bright solitons are negative and positive, respectively, for the corresponding parameters, which are shown in Fig. 1(b). It is clear that the solitons retain their shapes when moving. The above results indicate that our analytical solutions are in excellent agreement with the numerical results.

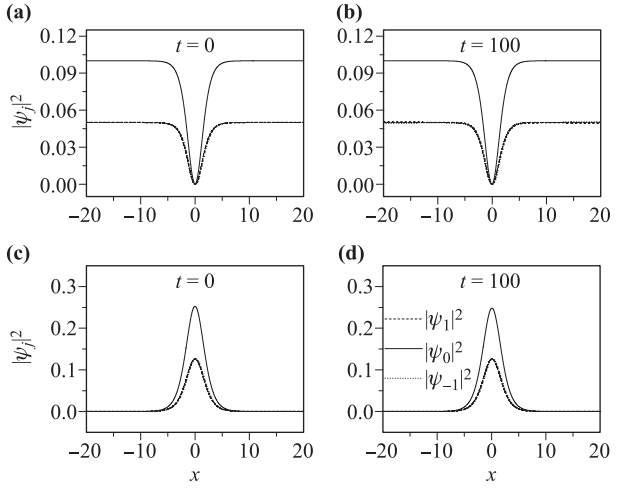

Fig. 3 Density profiles of stationary solitons. **(a, b)** Dark soliton for $\gamma = 8$, $\Omega = 70$ ($\Omega/\gamma^2 > \sqrt{2}/2$), $k = 0$, and $\theta = 0$, at time $t = 0$ and 100, respectively; **(c, d)** Bright soliton for $\gamma = 8$, $\Omega = 20$ ($\Omega/\gamma^2 < \sqrt{2}/2$), $k = 0$, $\kappa = 0$. $c_0 = 1$, $c_2 = -0.5$, $\varpi = 10$, and $\epsilon = 0.1$, at $t = 0$ and 100, respectively.

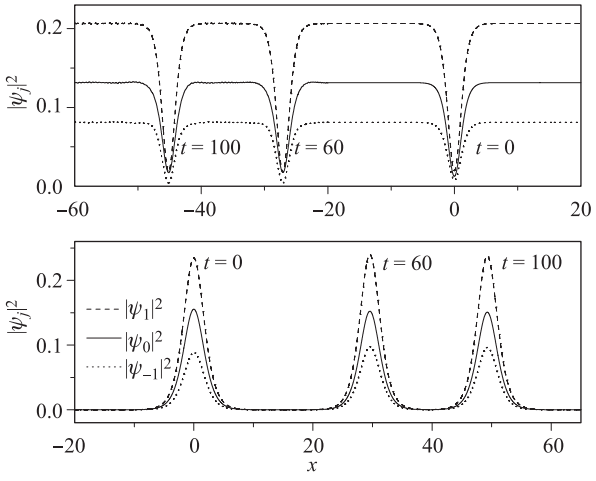

Fig. 4 Evolutionary profiles of moving solitons. Top panel: Moving dark soliton for $\gamma = 8$, $\Omega = 70$ ($\Omega/\gamma^2 > \sqrt{2}/2$), $k = -1.5$, $\theta = \pi/10$, and $\varpi = 20$. Bottom panel: Moving bright soliton for $\gamma = 8$, $\Omega = 20$ ($\Omega/\gamma^2 < \sqrt{2}/2$), $k = -0.5$, $\kappa = 1$, and $\varpi = 10$. Here, $c_0 = 1$, $c_2 = -0.5$, and $\epsilon = 0.1$.

4 Conclusion

Beginning with the 1D dimensionless GP equations for SOC spin-1 condensates, we have derived an effective nonlinear Schrödinger equation in free space via a multiscale perturbation method. This equation allows determination of different parameter spaces in which dark and bright solitons exist. Further, based on the analytical solution of this equation, we have obtained the approximate soliton solutions of the original GP equations. Both stationary and moving solitons (dark and bight) were found. We have numerically investigated those solutions, finding that all solitons are robust without distortion during propagation. In future, this analysis can be generalized to higher-dimensional cases, as well as the inhomogeneous case.

Acknowledgements This work was supported by the National Natural Science Foundation of China under Grant Nos. 11475027, 11764039, 11274255, and 11305132, the Natural Science Foundation of Gansu Province under Grant No. 17JR5RA076, and the Scientific Research Project of Gansu Higher Education under Grant No. 2016A-005.

References

1. M. R. Matthews, B. P. Anderson, P. C. Haljan, D. S. Hall, C. E. Wieman, and E. A. Cornell, Vortices in a Bose–Einstein condensate, *Phys. Rev. Lett.* 83(13), 2498 (1999)
2. J. Billy, V. Josse, A. Bernard, B. Hambrecht, P. Lugan,

D. Clement, L. Sanchez-Palencia, P. Bouyer, and A. Aspect, Direct observation of Anderson localization of matter waves in a controlled disorder, *Nature* 453(7197), 891 (2008)

3. G. Roati, C. D'Errico, L. Fallani, M. Fattori, C. Fort, M. Zaccanti, G. Modugno, M. Modugno, and M. Inguscio, Anderson localization of a non-interacting Bose–Einstein condensate, *Nature* 453(7197), 895 (2008)
4. S. Burger, K. Bongs, S. Dettmer, W. Ertmer, K. Sengstock, A. Sanpera, G. V. Shlyapnikov, and M. Lewenstein, Dark solitons in Bose–Einstein condensates, *Phys. Rev. Lett.* 83(25), 5198 (1999)
5. U. Al Khawaja, H. T. C. Stoof, R. G. Hulet, K. E. Strecker, and G. B. Partridge, Bright soliton trains of trapped Bose–Einstein condensates, *Phys. Rev. Lett.* 89(20), 200404 (2002)
6. G. Theocharis, D. J. Frantzeskakis, P. G. Kevrekidis, B. A. Malomed, and Y. S. Kivshar, Ring dark solitons and vortex necklaces in Bose–Einstein condensates, *Phys. Rev. Lett.* 90(12), 120403 (2003)
7. B. Wu, J. Liu, and Q. Niu, Controlled generation of dark solitons with phase imprinting, *Phys. Rev. Lett.* 88(3), 034101 (2002)
8. Y. Wu and L. Deng, Ultraslow optical solitons in a cold four-state medium, *Phys. Rev. Lett.* 93(14), 143904 (2004)
9. J. K. Xue, Interaction of ring dark solitons with ring impurities in Bose–Einstein condensates, *J. Phys. At. Mol. Opt. Phys.* 38(6), 671 (2005)
10. T. Taniuti and K. Nishihara, Nonlinear Waves, Pitman Advanced Publishing Program, 1983
11. A. C. Newell, Solitons in Mathematics and Physics, Society for Industrial and Applied Mathematics, 1987
12. S. Stellmer, C. Becker, P. Soltan-Panahi, E.M. Richter, S. Dörscher, M. Baumert, J. Kronjäger, K. Bongs, and K. Sengstock, Collisions of dark solitons in elongated Bose–Einstein condensates, *Phys. Rev. Lett.* 101(12), 120406 (2008)
13. H. G. Luo and W. M. Liu, Matter-wave solitons in heteronuclear atomic Bose–Einstein condensates with synchronously controllable interactions and potentials, *Phys. Rev. A* 84(5), 053631 (2011)
14. T. Busch and J. R. Anglin, Dark-bright solitons in inhomogeneous Bose–Einstein condensates, *Phys. Rev. Lett.* 87(1), 010401 (2001)
15. C. Hamner, J. J. Chang, P. Engels, and M. A. Hoefer, Generation of dark-bright soliton trains in superfluid–superfluid counterflow, *Phys. Rev. Lett.* 106(6), 065302 (2011)
16. K. Kasamatsu and M. Tsubota, Multiple domain formation induced by modulation instability in two-component Bose–Einstein condensates, *Phys. Rev. Lett.* 93(10), 100402 (2004)
17. P. G. Kevrekidis, D. J. Frantzeskakis, B. A. Malomed, and R. Carretero-González, Families of matter-waves in two-component Bose–Einstein condensates, *Eur. Phys. J. D* 28(2), 181 (2004)
18. T. W. Neely, E. C. Samson, A. S. Bradley, M. J. Davis, and B. P. Anderson, Observation of vortex dipoles in an oblate Bose–Einstein condensate, *Phys. Rev. Lett.* 104(16), 160401 (2010)
19. D. V. Freilich, D. M. Bianchi, A. M. Kaufman, T. K. Langin, and D. S. Hall, Real-time dynamics of single vortex lines and vortex dipoles in a Bose–Einstein condensate, *Science* 329(5996), 1182 (2010)
20. S. Middelkamp, P. J. Torres, P. G. Kevrekidis, D. J. Frantzeskakis, R. Carretero-González, P. Schmelcher, D. V. Freilich, and D. S. Hall, Guiding-center dynamics of vortex dipoles in Bose–Einstein condensates, *Phys. Rev. A* 84(1), 011605(R) (2011)
21. S. Wüster, T. E. Argue, and C. M. Savage, Numerical study of the stability of skyrmions in Bose–Einstein condensates, *Phys. Rev. A* 72(4), 043616 (2005)
22. T. Kawakami, T. Mizushima, M. Nitta, and K. Machida, Stable skyrmions in $SU(2)$ gauged Bose–Einstein condensates, *Phys. Rev. Lett.* 109(1), 015301 (2012)
23. Y. J. Lin, K. Jimenez-Garcia, and I. B. Spielman, Spin–orbit-coupled Bose–Einstein condensates, *Nature* 471(7336), 83 (2011)
24. V. Galitski and I. B. Spielman, Spin–orbit coupling in quantum gases, *Nature* 494(7435), 49 (2013)
25. X. O. Xu and J. H. Han, Emergence of chiral magnetism in spinor Bose–Einstein condensates with Rashba coupling, *Phys. Rev. Lett.* 108(18), 185301 (2012)
26. J. Radić, T. A. Sedrakyan, I. B. Spielman, and V. Galitski, Vortices in spin–orbit-coupled Bose–Einstein condensates, *Phys. Rev. A* 84(6), 063604 (2011)
27. X. F. Zhou, J. Zhou, and C. J. Wu, Vortex structures of rotating spin–orbit-coupled Bose–Einstein condensates, *Phys. Rev. A* 84(6), 063624 (2011)
28. C. Wang, C. Gao, C. M. Jian, and H. Zhai, Spin–orbit coupled spinor Bose–Einstein condensates, *Phys. Rev. Lett.* 105(16), 160403 (2010)
29. T. L. Ho and S. Zhang, Bose–Einstein condensates with spin–orbit interaction, *Phys. Rev. Lett.* 107(15), 150403 (2011)
30. T. Congy, A. M. Kamchatnov, and N. Pavloff, Nonlinear waves in coherently coupled Bose–Einstein condensates, *Phys. Rev. A* 93(4), 043613 (2016)
31. L. Salasnich and B. A. Malomed, Localized modes in dense repulsive and attractive Bose–Einstein condensates with spin–orbit and Rabi couplings, *Phys. Rev. A* 87(6), 063625 (2013)
32. V. Achilleos, D. J. Frantzeskakis, P. G. Kevrekidis, and D. E. Pelinovsky, Matter-wave bright solitons in spin–orbit coupled Bose–Einstein condensates, *Phys. Rev. Lett.* 110(26), 264101 (2013)

33. V. Achilleos, D. J. Frantzeskakis, P. G. Kevrekidis, P. Schmelcher, and J. Stockhofe, Positive and negative mass solitons in spin–orbit coupled Bose–Einstein condensates, *Rom. Rep. Phys.* 67(1), 235 (2015)
34. Y. V. Kartashov, V. V. Konotop, and F. Kh. Abdullaev, Gap solitons in a spin–orbit-coupled Bose–Einstein condensate, *Phys. Rev. Lett.* 111(6), 060402 (2013)
35. G. X. Huang, V. A. Makarov, and M. G. Velarde, Two-dimensional solitons in Bose–Einstein condensates with a disk-shaped trap, *Phys. Rev. A* 67(2), 023604 (2003)
36. S. Sinha, R. Nath, and L. Santos, Trapped two-dimensional condensates with synthetic spin–orbit coupling, *Phys. Rev. Lett.* 107(27), 270401 (2011)
37. H. Sakaguchi, B. Li, and B. A. Malomed, Creation of two-dimensional composite solitons in spin–orbit-coupled self-attractive Bose–Einstein condensates in free space, *Phys. Rev. E* 89(3), 032920 (2014)
38. V. E. Lobanov, Y. V. Kartashov, and V. V. Konotop, Fundamental, multipole, and half-vortex gap solitons in spin–orbit coupled Bose–Einstein condensates, *Phys. Rev. Lett.* 112(18), 180403 (2014)
39. Y. C. Zhang, Z. W. Zhou, B. A. Malomed, and H. Pu, Stable solitons in three dimensional free space without the ground state: Self-trapped Bose–Einstein condensates with spin–orbit coupling, *Phys. Rev. Lett.* 115(25), 253902 (2015)
40. D. L. Campbell, R. M. Price, A. Putra, A. Valdés-Curiel, D. Trypogeorgos, and I. B. Spielman, Magnetic phases of spin-1 spin–orbit-coupled Bose gases, *Nat. Commun.* 7, 10897 (2016)
41. L. Chen, H. Pu, and Y. Zhang, Spin–orbit angular momentum coupling in a spin-1 Bose–Einstein condensate, *Phys. Rev. A* 93(1), 013629 (2016)
42. S. Gautam and S. K. Adhikari, Phase separation in a spin–orbit-coupled Bose–Einstein condensate, *Phys. Rev. A* 90(4), 043619 (2014)
43. G. I. Martone, F. V. Pepe, P. Facchi, S. Pascazio, and S. Stringari, Tricriticalities and quantum phases in spin–orbit-coupled spin-1 Bose gases, *Phys. Rev. Lett.* 117(12), 125301 (2016)
44. Y. K. Liu and S. J. Yang, Exact solitons and manifold mixing dynamics in the spin–orbit coupled spinor condensates, *Europhys. Lett.* 108(3), 30004 (2014)
45. S. Gautam and S. K. Adhikari, Mobile vector soliton in a spin–orbit coupled spin-1 condensate, *Laser Phys. Lett.* 12(4), 045501 (2015)